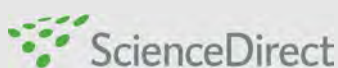
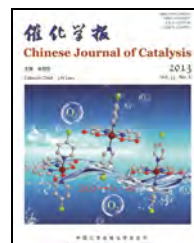


available at www.sciencedirect.com



journal homepage: www.elsevier.com/locate/chnjc

**Article****Molecularly imprinted polymer containing Fe(III) catalysts for specific substrate recognition**Wenqing Sun^a, Rong Tan^{a,*}, Weiguo Zheng^a, Donghong Yin^{a,b,#}^a*Institute of Fine Catalysis and Synthesis, Key Laboratory of Chemical Biology and Traditional Chinese Medicine Research (Ministry of Education), Hunan Normal University, Changsha 410081, Hunan, China*^b*Research and Development Center, China Tobacco Hunan Industrial Corporation, Changsha 410014, Hunan, China***ARTICLE INFO****Article history:**

Received 9 January 2013

Accepted 14 May 2013

Published 20 August 2013

Keywords:

Molecularly imprinted polymer

Iron(III) catalyst

Benzyl alcohol derivative

Catalytic oxidation

Substrate recognition

ABSTRACT

A series of molecularly imprinted polymers (MIPs) containing equal amounts of iron(III) were prepared by the polymerization of acrylamide and ethylene dimethacrylate in the presence of the template of *o*-, *m*-, or *p*-nitrobenzyl alcohol (NBA) and a FeCl_3 complex. The samples were characterized by scanning electron microscopy, N_2 adsorption, and Fourier transform infrared spectroscopy. The catalysts exhibited high catalytic activity and unique substrate recognition in the oxidation of benzyl alcohol derivatives in water using 30% H_2O_2 as the oxidant. The conversion of *p*-NBA was 80% over the *p*-Fe(III)-MIP catalyst when the template molecule was *p*-NBA, which had a good fit with the substrate. However, the conversion of *p*-NBA was less than 58% over *o*-Fe(III)-MIP or *m*-Fe(III)-MIP due to the mismatch of the substrate with the cavities of the Fe(III)-MIP. The results indicated that the Fe(III)-MIP samples contained molecular recognizable shapes and sites in their cavities that match the corresponding substrate. The special recognizing cavities of the Fe(III)-MIP catalyst exhibited unique substrate recognition, and therefore the selectivity for the substrate was improved.

© 2013, Dalian Institute of Chemical Physics, Chinese Academy of Sciences.
Published by Elsevier B.V. All rights reserved.

1. Introduction

Molecularly imprinted polymers (MIPs) with binding sites complementary to the imprint molecule in terms of the shape and position of the functional groups are of interest in the fields of chiral stationary phases, solid phase extraction, mimetic enzyme catalysts, controlled release of drug, and membrane separation technology [1]. To fabricate MIPs, functional monomers and templates are first allowed to form a self-organized architecture using covalent, non-covalent, or complex self-assembly. Polymerization in the presence of a cross linker is then performed to fix the self-organized architecture. The subsequent removal of the template from the polymeric matrix

leaves behind an imprinted cavity with a recognizing ability for the imprint species [2–4]. Known as the “template’s memory”, molecular imprinting can be a promising technique to acquire a catalyst that specifically recognizes special reactants because it should be possible to mimic the shape of the templates by imprinting and also at the same time introduce suitable catalytic groups and binding sites into the active sites in a predetermined orientation. Therefore, constructing a catalytically active center with a special structure and function in MIP imprinted cavities would open up new ways for the design of highly active and highly selective new catalysts [5–8].

Metal ions are commonly introduced into the MIP imprinted cavities for the fabrication of molecularly imprinted catalysts

*Corresponding author. Tel: +86-731-88872576; Fax: +86-731-88872531; E-mail: yiyangtanrong@126.com

#Corresponding author. Tel: +86-731-88872576; Fax: +86-731-88872531; E-mail: yindh@hunnu.edu.cn

This work was supported by the National Natural Science Foundation of China (21003044, 20973057), the Natural Science Foundation of Hunan Province (10JJ6028), and the Program for Science and Technology Innovative Research Team in Higher Educational Institutions of Hunan Province.

DOI: 10.1016/S1872-2067(12)60624-X | http://www.sciencedirect.com/science/journal/18722067 | Chin. J. Catal., Vol. 34, No. 8, August 2013

(MICs). By assembling with a metal as the pivot, the monomer and template are bridged through coordination binding [9]. This provides higher fidelity of the imprinted material and therefore improves the specific recognition of imprinted species [10,11]. Hence, research in molecularly imprinted polymer catalysts containing metal ions has practical importance.

The selective oxidation of benzyl alcohol derivatives to the corresponding aldehyde compounds is an important reaction in fine chemicals and organic synthesis [12]. Traditionally, dilute nitric acid is used to catalyze the reaction to give the corresponding aldehyde compounds, but equipment corrosion and environmental pollution are inevitable in the process [13,14]. Therefore, it is desirable to develop a novel green and environmentally benign catalyst for the oxidation. Based on the excellent performance of Fe(III) in the selective oxidation reaction with H₂O₂ as oxidant [15,16], and the effect of the metal ion for stabilizing the MICs and regulating the reactivity, a series MIPs containing equal amounts of Fe(III) were prepared by the polymerization of acrylamide and ethylene dimethacrylate in the presence of the template of *o*-, *m*-, or *p*-nitrobenzyl alcohol (NBA) and a FeCl₃ complex. The catalytic performance of the MICs was investigated in the oxidation of benzyl alcohol derivatives in water using H₂O₂ as the oxidant. The MICs exhibited high catalytic activities and unique substrate recognition in the oxidation due to the high binding affinity of the active sites and the “template’s memory” of the imprinted cavity.

2. Experimental

2.1. Preparation of Fe(III)-MIP

o-NBA, *m*-NBA, *p*-NBA, acrylamide (AM), divinyl benzene, and ethylene glycol dimethacrylate (EGDMA) were obtained from Alfa Aesar. Ferric chloride, azobisisobutyronitrile (AIBN), dimethyl sulfoxide (DMSO), and toluene were laboratory grade reagents from local suppliers. All solvents were purified by standard procedures before use.

The preparation of Fe(III)-MIPs with different template molecules is outlined in Scheme 1. Anhydrous FeCl₃ (0.525 mmol) and *o*-NBA (0.75 mmol) were dissolved in a mixture of toluene (5 ml) and DMSO (5 ml). AM (3 mmol), EGDMA (15 mmol), and AIBN (0.1 g) were then added and the mixture was given an ultrasonic treatment. The resulting solution was purged with dry N₂ for 15 min. Polymerization was performed at 60 °C for 24 h under vacuum. The solvents were removed and the polymer was ground and sieved to yield particles in the size range of 50–60 µm. The solids were decanted from acetone (10 ml) three times. The polymer was Soxhlet extracted with a

mixture of methanol and acetic acid (9/1, v/v) until the template molecule was completely removed, and the polymer was dried under vacuum at 40 °C. The powder obtained was denoted as *o*-Fe(III)-MIP. The MICs of *m*-Fe(III)-MIP and *p*-Fe(III)-MIP were also prepared by the above similar preparation procedure. The Fe(III) content in the prepared catalysts was 0.3 mmol/g, which was measured by complexometry.

For comparison, the blank non-imprinted polymer (denoted as NIP) and non-imprinted polymer containing Fe(III) ion (denoted as Fe-(III)NIP) were also prepared by a similar preparation procedure to Fe(III)-MIP except for the addition of the template molecule. The Fe(III) content in the Fe(III)-NIP was calculated to be 0.3 mmol/g from the complexometry result.

2.2. Determination of the Fe content

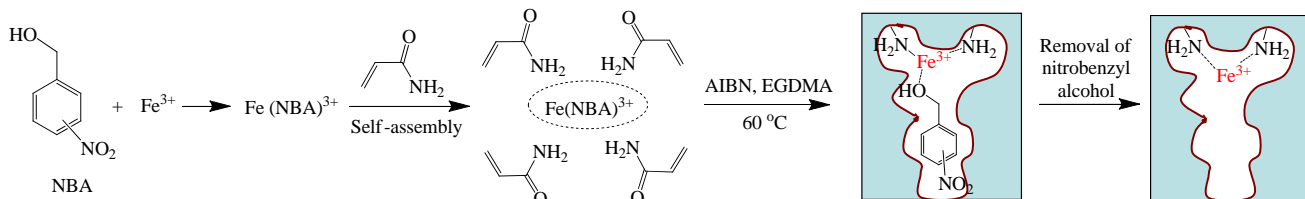
The catalyst (~0.1 g) was calcined at 500–600 °C for 5 h to remove the organic components in the catalyst. The residue was transferred to a conical flask, treated with aqua regia (4 ml), and boiled to dry three times. The mixture was dissolved in distilled water (5 ml) and added into the glycine-hydrochloric acid buffer solution (10 ml). The pH value of the solution was adjusted to 2–3 by the addition of sulfosalicylic acid (5 drops, 100 g/L). The resulting solution was heated to 60 °C. The wine colored solution was titrated with EDTA (0.01 mol/L) until the solution was colorless. The Fe(III) ion content was determined from the average value of three repeated measurements [16].

2.3. Detection of the template-monomer interaction and the intervention of FeCl₃

The template molecule (2.5 ml) was placed into a sample cell of the UV-vis spectrometer, and then the functional monomer (100 µl) was added repeatedly at room temperature. The change of the UV absorption bands after each addition was used to detect if there was template-monomer interaction. The template-FeCl₃ interaction and monomer-FeCl₃ interaction were also detected by a similar method [17].

2.4. Characterization

The morphology of the samples was observed by using a JSM-6360LV scanning electron microscope (SEM). The N₂ adsorption-desorption experiments were performed at –196 °C on a Micromeritics TriStar 3000 sorptometer. The sample was degassed under 1.33 × 10^{–3} Pa at 80 °C overnight before measurement. The analytical data were processed by the BET equation for surface area and by the BJH model for pore size distri-



Scheme 1. Preparation of the Fe(III)-MIP catalyst.

bution. Fourier transform infrared spectra (FT-IR) were obtained using KBr with a resolution of 2 cm^{-1} and scans in the range $400\text{--}4000\text{ cm}^{-1}$ using an AVATAR 370 spectrophotometer. UV-vis spectra were recorded on a Perkin Elmer Lambda 19 UV-vis spectrophotometer in the range $200\text{--}600\text{ nm}$.

2.5. Catalyst testing

In a typical experiment, Fe(III)-MIP (0.1 g), benzyl alcohol derivatives (1.8 mmol), and deionized water (15 ml) were charged in a 50 ml round bottom flask. The pH value was adjusted to 2. The mixture was heated to 80°C under continuous stirring. H_2O_2 (5 ml) containing 0.75 ml of H_2O_2 (30 wt%) was added dropwise to the above mixture at a rate of 0.1 ml/min. After the reaction, the mixture was cooled to room temperature. The reaction products were extracted with ethyl ether and dried with anhydrous Na_2SO_4 . The products were analyzed by an Agilent 6890N gas chromatograph (HP-624 capillary column, $30\text{ m} \times 0.25\text{ mm}$) with a flame ionization detector (FID) using N_2 as carrier gas and were further identified by GC-MS using an HP 5790 series mass selective detector.

3. Results and discussion

3.1. Design of the Fe(III)-MIP

The molecular self-assembly of template-monomers is a prerequisite for the fabrication of imprinting. Normally, depending on the monomer-template interaction, the imprint is achieved by arranging polymerizable monomers around a guidable template. By assembling with a metal as the pivot, the monomer and template are bridged through coordination binding.

Taking the design of *p*-Fe(III)-MIP for example, Fig. 1(a) presents the observed UV-vis spectra used to monitor the *p*-NBA- FeCl_3 interaction. Using the mole proportion recipe in Section 2.3 as the control and an initial point, FeCl_3 and *p*-NBA were mixed. As shown in Fig. 1(a), the mixture containing equal amounts of FeCl_3 and *p*-NBA showed a characteristic band at 285 nm. The addition of more *p*-NBA resulted in a shift of the

UV absorption band with increasing absorbance. The shift increased with an increase in the added amount. The shift in the absorption band reached a maximum (290 nm) when the added *p*-NBA reached a critical value (corresponding to 5:1 of *p*-NBA:Fe(III) molar ratio). Beyond the critical value, there was no additional shift and only an increasing absorbance of the absorption band was observed. These observations strongly indicated an interaction existing between *p*-NBA and FeCl_3 and that the interaction was subsequently saturated by the adding of the quintuple amount of *p*-NBA.

Figure 1(b) presents the observation of UV-vis spectra to monitor the AM- FeCl_3 interaction. Using the mole proportion recipe in Section 2.3 as the control and an initial point, AM and FeCl_3 were mixed. As shown in Fig. 1(b), the mixture containing AM and FeCl_3 (2/1) showed a characteristic band at 271 nm. An increase in the added amount of AM also resulted in a shift of UV absorption band and increasing absorbance. The shift in the absorption band achieved a maximum (274 nm) when the added AM reached a critical value (corresponding to 8:1 of AM:Fe(III) molar ratio). Beyond the critical value, no additional shift but only an increasing absorbance in the absorption band was observed. These observations strongly indicated an interaction existing between AM and FeCl_3 and that the interaction was subsequently saturated by adding a stoichiometric amount of AM.

The interaction between AM and *p*-NBA was also followed by UV-vis spectra as shown in Fig. 1(c). Using the mole proportion recipe in Section 2.3 as the control and an initial point, the monomer and template were mixed. The mixture containing equal amounts of AM and *p*-NBA showed a characteristic band at 216 nm. Addition of AM resulted in a red shift of the UV absorption band and increasing absorbance. The shift in the absorption bands achieved a maximum (219 nm) when added AM reached a critical value (corresponding to 4:1 of AM:*p*-NBA molar ratio). Beyond the critical value, there was no additional shift and only an increasing absorbance in the absorption band was observed. It is the evidence that there is an interaction between AM and *p*-NBA and that the interaction was subsequently saturated by adding a stoichiometric amount of AM.

Therefore, there were interactions between the monomer

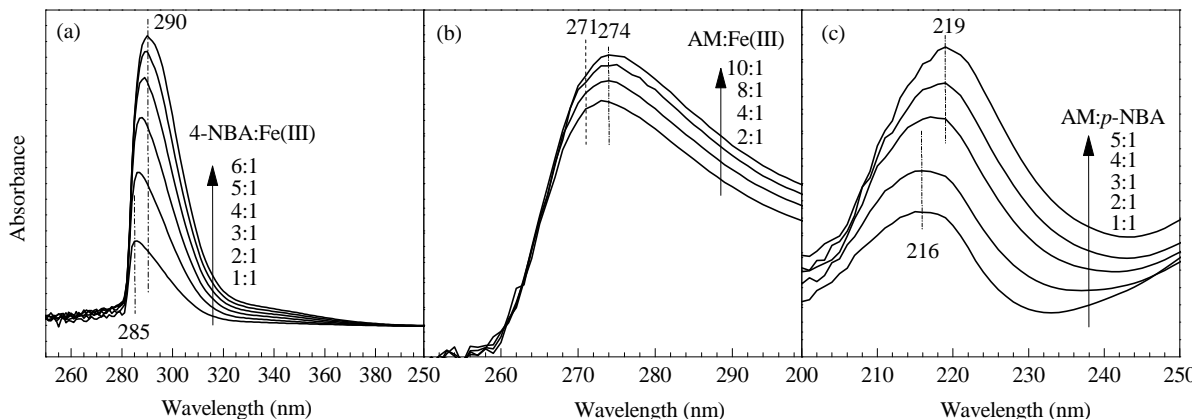


Fig. 1. UV-vis spectra of FeCl_3 with the addition of *p*-NBA (a), of FeCl_3 with the addition of AM (b), and of *p*-NBA with the addition of AM (c) at different molar ratios.

and metal, the template and metal, and between the monomer and template, and the interactions were saturated by adding a stoichiometric amount of monomer or template. Too much assembled monomer will give the binding framework a spatial and steric mismatch with the template due to an over abundance of functional groups (binding sites) that are distributed randomly throughout the polymer. Too low an amount of assembled monomer will give a polymer with an insufficient quantity of functional groups to achieve complete self-assembly. Thus, for the rational design of a highly specific imprint, a stoichiometric amount of monomer is necessary. According to the basic recipe (Section 2.1), 3 mmol of AM was employed to synthesize these polymers. The *p*-NBA (0.75 mmol) was thus used to be in accord with the stoichiometric saturated value (4:1 of AM:*p*-NBA molar ratio). Based on the linkage of the pivot, FeCl₃ (0.525 mmol) is therefore required to achieve complete self-assembly (i.e., the sum of (monomer/8) and (template/5)). With this recipe, one can expect to get a binding framework capable of stoichiometrically binding the imprint species. This is a prerequisite for the preparation of highly specific imprints.

3.2. Characterization of the samples

3.2.1. SEM results

Figure 2 presents SEM images of the *p*-Fe(III)-MIP and Fe(III)-NIP catalysts and the blank NIP. There were some cavities existing within *p*-Fe(III)-MIP. From the preparation process, these would be a consequence of imprinting. Using metal as a pivot, the weak linkage between the monomer and template now becomes a stronger coordination binding. After this was fixed by polymerization, an imprint with a higher fidelity was thus left behind. Furthermore, the obvious surface cavities may be a result of the irregular accumulation of amorphous MIP due to the participation of FeCl₃ and *p*-NBA during the polymerization. As expected, the absence of the template molecule in the polymerization led to less and smaller cavities within the Fe(III)-NIP sample (Fig. 2(b)). The blank polymer (NIP) presented a relatively smooth surface (Fig. 2(c)). Regarding the difference between the imprinted materials, it is helpful to note the pivot role of the Fe(III) ion in the preparation process. As a result, the Fe(III)-MIP catalyst can be expected to display a higher specificity for the hydrolysis of the imprint species. The imprinted cavity structure of the

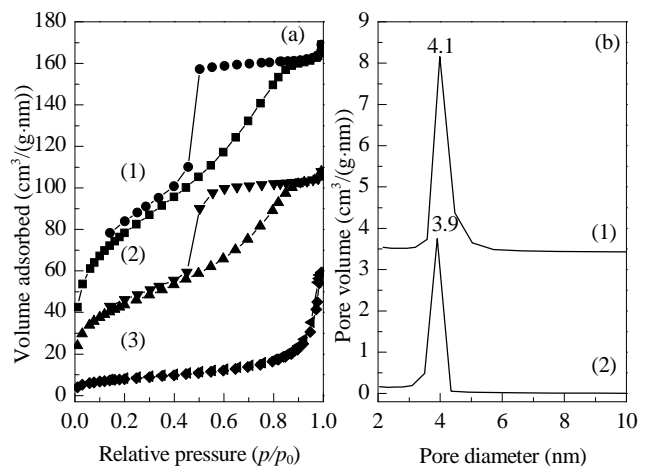


Fig. 3. Nitrogen adsorption isotherms (a) and pore size distribution (b) of *p*-Fe(III)-MIP (1), Fe(III)-NIP (2), and NIP (3).

p-Fe(III)-MIP sample was also confirmed by N₂ adsorption isotherms.

3.2.2. N₂ adsorption isotherms

N₂ adsorption isotherms that recorded the textural properties of *p*-Fe(III)-MIP, Fe(III)-NIP, and NIP are shown in Fig. 3. The samples of *p*-Fe(III)-MIP and Fe(III)-NIP displayed typical type IV isotherms with a clear adsorption-desorption hysteresis loop at $0.4 < p/p_0 < 0.8$. The adsorption capacities of the two samples increased dramatically at lower relative pressures ($p/p_0 < 0.4$), indicating the presence of micropores (diameter < 1.9 nm). The typical hysteresis loop at $0.4 < p/p_0 < 0.8$ in the N₂ adsorption isotherms of *p*-Fe(III)-MIP and Fe(III)-NIP indicated the existence of some mesoporosity in the samples [18,19], which resulted in capillary condensation and further increased the adsorption capacity. At high relative pressure ($p/p_0 > 0.9$), the adsorption capacities increased rapidly, which was probably due to the mesoporosity from the accumulation of amorphous MIP. Meanwhile, the N₂ adsorption isotherm showed that there were no structural channels in blank NIP. The textural properties of *p*-Fe(III)-MIP, Fe(III)-NIP, and NIP are listed in Table 1. As expected, in comparison to Fe(III)-NIP, *p*-Fe(III)-MIP possessed increased surface area, pore size, and pore volume. In particular, the surface area of *p*-Fe(III)-MIP was almost twice as large as that of Fe(III)-NIP. The results further confirmed that the intimate participation of FeCl₃ and

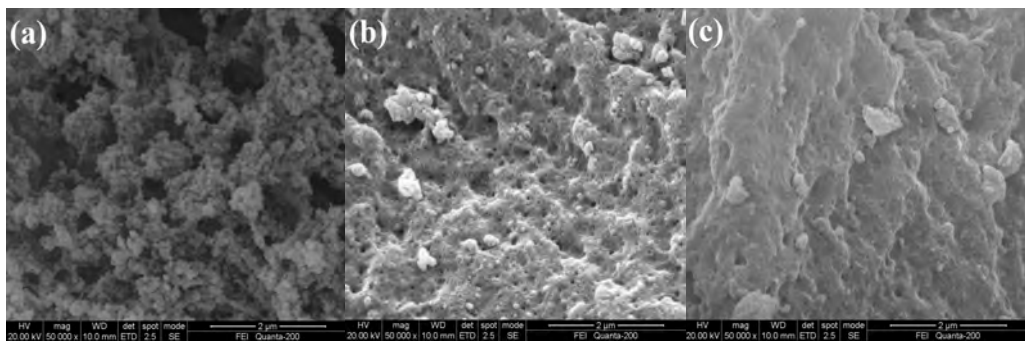


Fig. 2. SEM images of *p*-Fe(III)-MIP (a), Fe(III)-NIP (b), and NIP (c).

Table 1

Textural parameters of the samples.

Sample	$A_{\text{BET}}/(\text{m}^2/\text{g})$	D/nm	$V/(\text{cm}^3/\text{g})$
<i>p</i> -Fe(III)-MIP	269	4.1	0.25
Fe(III)-NIP	149	3.9	0.17
NIP	27	—	0.09

p-NBA during the polymerization that resulted in the imprinted cavities in the *p*-Fe(III)-MIP sample, which is consistent with SEM results.

3.2.3. FT-IR results

The *p*-Fe(III)-MIP, Fe(III)-NIP, and NIP samples were characterized by FT-IR spectroscopy. As shown in Fig. 4, beyond the fingerprint area, there were three main absorption bands in the spectra in the ranges of 3400–3700, 2700–3200, and 1500–1800 cm^{-1} , which can be assigned to the stretching of N–H/C–H, C=N, and C–N, respectively [20]. The absorption bands in the fingerprint area were from the C–C stretch [21]. The spectra of *p*-NBA and catalyst precursor with *p*-NBA are also presented in Fig. 4 for comparison. As observed, the template molecule of *p*-NBA displayed the O–H stretching band at 3510 cm^{-1} , while this absorption band was shifted to 3443 cm^{-1} in the spectrum of the catalyst precursor, which confirmed the formation of coordination binding between the hydroxyl group (–OH) of *p*-NBA and the metal ion in the catalyst precursor. After Soxhlet extraction with a mixture of methanol and acetic acid (9/1, v/v), this characteristic absorption band associated with *p*-NBA was dramatically decreased to almost the same intensity as that of the blank polymer. The results showed that the template molecule of *p*-NBA was eluted, leaving behind the intact Fe(III)-MIP sample with the specific imprinted cavities.

3.3. Catalytic activity of the catalysts

3.3.1. Oxidation of single nitrobenzyl alcohol

Table 2 summarizes the catalytic activity of the synthesized NIP, Fe(III)-NIP, and the *o*-, *m*-, *p*-Fe(III)-NIP catalysts in the oxidation of benzyl alcohol derivatives in water using 30%

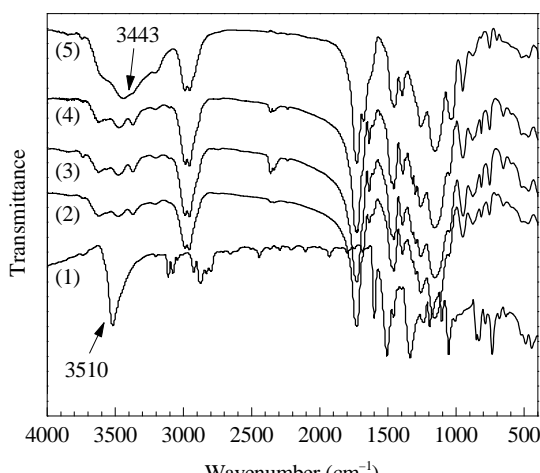


Fig. 4. FT-IR spectra of *p*-NBA (1), NIP (2), Fe(III)-NIP (3), *p*-Fe(III)-MIP (4), and *p*-Fe(III)-MIP precursor (5).

Table 2

Oxidation of nitrobenzyl alcohol over the different catalysts.

Catalyst	Conversion (%)		
	<i>o</i> -NBA	<i>m</i> -NBA	<i>p</i> -NBA
—	trace	trace	trace
NIP	< 5.0	< 5.0	< 5.0
<i>o</i> -Fe(III)-MIP	65	37	51
<i>m</i> -Fe(III)-MIP	39	69	58
<i>p</i> -Fe(III)-MIP	36	42	80
Fe(III)-NIP	34	33	49

Reaction conditions: catalyst 0.1 g, substrate 1.8 mmol, 30% H_2O_2 0.75 ml, H_2O 15 ml, 80 °C, 4 h.

H_2O_2 as the oxidant. As shown in Table 2, there was no conversion of nitrobenzyl alcohol without a catalyst or with the NIP. The conversion of the benzyl alcohol derivatives to the corresponding benzaldehyde increased significantly when Fe(III)-NIP or Fe(III)-MIP was used as the catalyst, indicating the need for the Fe(III) ion under the conditions employed here. It is noteworthy that the Fe(III)-MIP catalyst exhibited specific substrate recognition in the oxidation. When *o*-NBA was used as the substrate, the *o*-Fe(III)-MIP catalyst showed the highest activity with 65% conversion within 4 h at 80 °C. However, *m*-Fe(III)-MIP, *p*-Fe(III)-MIP, and Fe(III)-NIP were far less active compared to *o*-Fe(III)-MIP, and they gave only 34%–39% conversion under the same conditions. The difference in catalytic activity is related to the imprinted cavity structure of the Fe(III)-MIP samples. *o*-Fe(III)-MIP, with imprinted cavities complementary to *o*-NBA in terms of the shape and position of functional groups, showed a substantially increased affinity for *o*-NBA, which therefore enhanced the reactivity [22,23]. While, the less suitable fit in shape and structure between *o*-NBA and the imprinted cavities in *m*-Fe(III)-MIP, *p*-Fe(III)-MIP, and Fe(III)-NIP resulted in less efficient catalysts in the oxidation. The *m*-Fe(III)-MIP sample was also found to exhibit the highest activity in the oxidation of *m*-NBA, affording 69% conversion. Only 33%–42% conversion were obtained with *o*-Fe(III)-MIP, *p*-Fe(III)-MIP, or Fe(III)-NIP as catalysts. Likewise, *p*-Fe(III)-MIP showed the highest activity in the oxidation of the *p*-NBA due to the better affinity with *p*-NBA. The results confirmed that constructing the catalytic active center with a specific structure and function in the imprinted cavities of the MIPs endowed the polymer with catalytic activity and specific substrate recognition. The imprinted cavities in the MIC were responsible for the substrate recognition and the accelerated reaction rate. As expected, non-specific substrate recognition was observed with Fe(III)-NIP in the oxidation of *o*-, *m*-, and *p*-NBA due to the absence of imprinted cavities.

3.3.2. Oxidation of mixed nitrobenzyl alcohol

To provide further insight into the specific substrate recognition of the Fe(III)-MIP samples, comparative reaction studies were performed using mixed *o*-, *m*-, and *p*-NBA as the substrate. The results are summarized in Table 3. The Fe(III)-MIP samples showed highly specific substrate recognition and catalysis towards the imprint species during the oxidation. When *o*-Fe(III)-MIP was used as the catalyst, *o*-NBA had the highest conversion of the benzyl alcohol derivatives in the mixed sub-

Table 3

Oxidation of mixed nitrobenzyl alcohol over the different catalysts.

Catalyst	Conversion (%)		
	<i>o</i> -NBA	<i>m</i> -NBA	<i>p</i> -NBA
<i>o</i> -Fe(III)-MIP	70	28	31
<i>m</i> -Fe(III)-MIP	27	72	32
<i>p</i> -Fe(III)-MIP	29	40	85

Reaction conditions: catalyst 0.1 g, mixed nitrobenzyl alcohols (0.6 mmol *o*-NBA, 0.6 mmol *m*-NBA, and 0.6 mmol *p*-NBA) 1.8 mmol, 30% H₂O₂ 0.75 ml, H₂O 15 ml, 80 °C, 4 h.

strates. The 70% conversion of *o*-NBA was obtained within 4 h at 80 °C. This can be explained by that the structure of *o*-NBA is complementary to the imprinted cavities and binding sites of *o*-Fe(III)-MIP in terms of the shape and position of the functional groups. A mismatch effect was observed for *m*-NBA and *p*-NBA, and only 28% and 31% conversions were obtained, respectively. Also, *m*-NBA was the most reactive of the benzyl alcohol derivatives in the mixed substrates when *m*-Fe(III)-MIP was used as the catalyst. Moreover, *p*-Fe(III)-MIP was more reactive toward *p*-NBA due to a greater affinity. These results provided further evidence for the specific substrate recognition of the Fe(III)-MIPs.

3.3.3. Influence of reaction time

The reaction time played an important effect on the specific substrate recognition of the Fe(III)-MIPs. The relationship between reaction time and specific substrate recognition of the *o*-, *m*-, and *p*-Fe(III)-MIP in the oxidation of benzyl alcohol derivatives was investigated. The results are illustrated in Fig. 5. In general, a prolonged reaction time favored high conversion as well as specific substrate recognition. The best imprinting effect for all the Fe(III)-MIPs was observed at 4 h. When *o*-NBA was used as the substrate, the *o*-Fe(III)-MIP exhibited much higher activity, affording 65% conversion at 4 h, while the conversion of *o*-NBA over *m*-Fe(III)-MIP or *p*-Fe(III)-MIP was negligible. The imprinting factors of *m*-Fe(III)-MIP and *p*-Fe(III)-MIP (ratio of the catalysis by *o*-Fe(III)-MIP compared to *m*-Fe(III)-MIP and *p*-Fe(III)-MIP) are 1.67 and 1.81, respectively. The imprinting factor decreased with prolonged reaction time although the conversion of *o*-NBA increased. The reduced imprinting effect would be due to the access of the mismatched

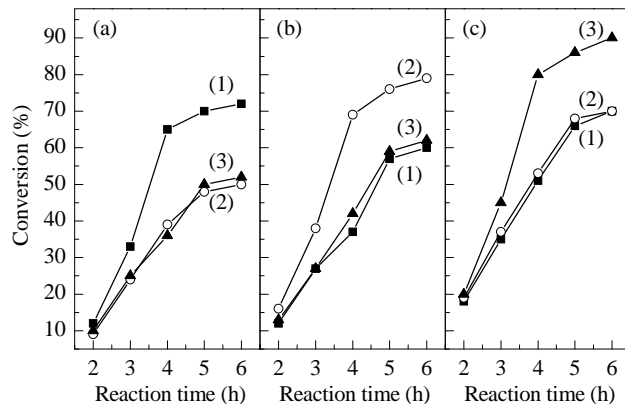


Fig. 5. Effect of reaction time on the oxidation of *o*-NBA (a), *m*-NBA (b), and *p*-NBA (c) over catalysts *o*-Fe(III)-MIP (1), *m*-Fe(III)-MIP (2), and *p*-Fe(III)-MIP (3).

substrate into the imprinted cavities in the oxidation after prolonged reaction time. A similar effect of reaction time on the specific substrate recognition of the Fe(III)-MIPs was also observed in the oxidation of *m*-NBA and *p*-NBA (Fig. 5(b) and (c)). The results further confirmed that the molecular recognition and specific catalysis by Fe(III)-MIPs is a result of shape and structure complementarity between the imprinted cavities and substrate.

4. Conclusions

Highly substrate-selective Fe(III)-MIPs were prepared by using the templates of *o*-, *m*-, or *p*-NBA and a ferric(III) trichloride complex. By combining a template-imprinted memory with Fe(III) ion active sites, the polymer catalysts showed highly specific molecular recognition and catalysis toward the imprint species in the oxidation of benzyl alcohol derivatives in water with 30% H₂O₂. Therefore, the molecular imprinting technique offers potential for developing tailored catalysts for special substrates.

References

- [1] Petcu M, Karlsson J P, Whitcombe M J, Nicholls I A. *J Mol Recognit*,

Graphical Abstract

Chin. J. Catal., 2013, 34: 1589–1598 doi: 10.1016/S1872-2067(12)60624-X

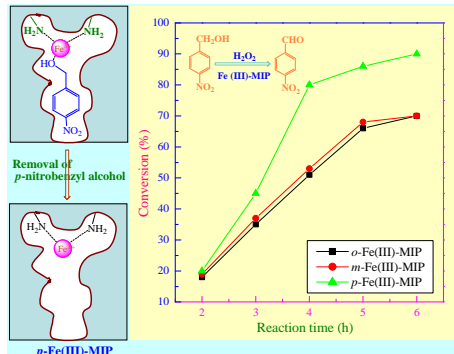
Molecularly imprinted polymer containing Fe(III) catalysts for specific substrate recognition

Wenqing Sun, Rong Tan*, Weiguo Zheng, Donghong Yin*

Hunan Normal University;

Tobacco Hunan Industrial Corporation

A series of molecularly imprinted polymers (MIPs) containing the equal amount of iron(III) were found to be the specific substrate recognition catalysts in the oxidation of substituted benzyl alcohol in water.



- 2009, 22: 18
- [2] Haupt K, Dzgoev A, Mosbach K. *Anal Chem*, 1998, 70: 628
- [3] Andersson L, Sellergren B, Mosbach K. *Tetrahedron Lett*, 1984, 25: 5211
- [4] Matsui J, Nicholls I A, Takeuchi T, Mosbach K, Karube I. *Anal Chim Acta*, 1996, 335: 71
- [5] Brunkan N M, Gagné M R. *J Am Chem Soc*, 2000, 122: 6217
- [6] Li Y Z, Fan Y N, Yang H P, Xu B L, Feng L Y, Yang M F, Chen Y. *Chem Phys Lett*, 2003, 372: 160
- [7] Tang Z C, Li Q Y, Lu G X. *Carbon*, 2007, 45: 41
- [8] Li S J, Gong S Q. *Adv Funct Mater*, 2009, 19: 2601
- [9] Guo J J, Cai J B, Su Q D. *J Rare Earths*, 2009, 27: 22
- [10] Liu H X, Yue H, Li S J, Li W K. *J Inorg Organomet Polym Mater*, 2009, 19: 335
- [11] Tada M, Iwasawa Y. *J Mol Catal A*, 2003, 199: 115
- [12] Hashmi A S K. *Chem Rev*, 2007, 107: 3180
- [13] Yadav G D, Mistry C K. *J Mol Catal A*, 2001, 172: 135
- [14] Liu C, Tan R, Yu N Y, Yin D H. *Microporous Mesoporous Mater*, 2010, 131: 162
- [15] Liu C B, Ye X K, Wu Y. *Chin J Catal* (刘诗标, 叶兴凯, 吴越. 催化学报), 1997, 18: 140
- [16] Lan W, Zhong S, Fu Z H. *Ind Catal (China)* (兰婉, 裴敏, 伏再辉. 工业催化), 2008, 116: 52
- [17] Li S J, Tong K J, Zhang D N, Huang X. *J Inorg Organomet Polym Mater*, 2008, 18: 264
- [18] Liu C, Tan R, Sun W Q, Yin D H. *Chin J Catal* (刘成, 谭蓉, 孙文庆, 银董红. 催化学报), 2012, 33: 1032
- [19] Peng L, Yu N Y, Tang Q L, Qiu H Y, Yin D L, Yin D H. *Acta Phys-Chim Sin*, 2007, 23: 1572
- [20] Li S J, Liao C, Li W K, Chen Y F, Hao X. *Macromol Biosci*, 2007, 7: 1112
- [21] Zhang D N, Li S G, Li W K, Chen Y F. *Catal Lett*, 2007, 115: 169
- [22] Hoshino Y, Koide H, Urakami T, Kanazawa H, Kodama T, Oku N, Shea K J. *J Am Chem Soc*, 2010, 132: 6644
- [23] Zhu Z K, Tan R, Sun W Q, Yin D H. *Chin J Catal* (祝贞科, 谭蓉, 孙文庆, 银董红. 催化学报), 2011, 32: 1508

分子印迹聚合物负载Fe(III)催化剂的底物识别性能

孙文庆^a, 谭蓉^{a,*}, 郑卫国^a, 银董红^{a,b,#}

^a湖南师范大学精细催化合成研究所, 化学生物学和中药分析教育部重点实验室, 湖南长沙410081

^b湖南中烟工业有限责任公司技术研发中心, 湖南长沙410014

摘要: 分别以 o -、 m -和 p -硝基苯甲醇与 FeCl_3 的配合物为模板分子, 丙烯酰胺为功能单体, 二甲基丙烯酸乙二醇酯为交联剂, 采用本体聚合法制备了三种Fe(III)含量相同的分子印迹聚合物(MIP) o -Fe(III)-MIP, m -Fe(III)-MIP和 p -Fe(III)-MIP。并采用扫描电镜、 N_2 吸附-脱附及红外光谱等方法对催化剂结构进行了表征。在以水为溶剂, 过氧化氢(30%)为氧化剂的苯甲醇衍生物氧化反应中, 该类催化剂表现出优异的催化活性和独特的底物识别性能。当以 p -Fe(III)-MIP为催化剂时, p -硝基苯甲醇的转化率达到80%, 而在其他两个催化剂上均低于58%。这表明Fe(III)-MIP催化剂结构中具有与底物分子匹配的印迹空腔与识别位点, 对底物分子表现出专一识别性, 因而提高了催化剂对底物的选择性。

关键词: 分子印迹聚合物; 铁(III)催化剂; 苯甲醇衍生物; 催化氧化; 底物识别

收稿日期: 2013-01-09. 接受日期: 2013-05-14. 出版日期: 2013-08-20.

*通讯联系人. 电话: (0731)88872576; 传真: (0731)88872531; 电子信箱: yiyangtanrong@126.com

#通讯联系人. 电话: (0731)88872576; 传真: (0731)88872531; 电子信箱: yindh@hunnu.edu.cn

基金来源: 国家自然科学基金(21003044, 20973057); 湖南省自然科学基金(10JJ6028); 湖南省教育厅高校科技创新团队。

本文的英文电子版由Elsevier出版社在ScienceDirect上出版(<http://www.sciencedirect.com/science/journal/18722067>)。

1. 前言

分子印迹聚合物(MIP)是一种在空间结构和结合位点上与印迹分子具有完全互补结构空穴的聚合物^[1], 在手性固定相、仿生传感器、固相萃取、模拟酶催化、药物控释及膜分离技术等领域表现出良好的应用前景。其印迹空穴通过共价键、非共价键或金属配位等方式选择性地结合模板分子^[2-4], 达到分子识别目的。利用分子印迹技术制备具有催化活性的分子印迹聚合物催化剂(MIC), 不仅可以通过选用适当的模板构建具有专一识别性能的印迹空穴, 而且可以通过选用适当的单体在空穴内构建出与底物匹配的结合位点以及起催化作用的活性基团, 使催化剂表现出高活性和高选择性。因此, 在

MIP印迹空腔内构建具有特殊结构和功能的催化活性中心, 为设计高活性和高选择性的新型催化剂开辟了一条新途径^[5-8]。

在功能单体与模板分子预组装中, 金属离子可作为桥梁起到支撑中心的作用^[9], 限制了分子段链因热运动形成的模板构像的偏离, 可有效地提高印迹材料的保真度, 使分子印迹催化剂既具有催化剂高活性的优点, 又具有对底物或反应产物专一识别的功能, 从而提高催化活性和选择性^[10,11]。因此, 研究分子印迹聚合物负载的金属催化剂及其底物识别性对提高催化剂活性和选择性具有重要的理论意义和应用价值。

苯甲醇衍生物选择性氧化生成相应的醛基化合物是精细化学品和有机中间体合成中的重要反应^[12], 其合

成方法备受关注^[13,14]。传统工艺大多采用稀硝酸为催化剂, 生产中存在严重的设备腐蚀和环境污染问题, 研发新型绿色环保催化剂及对环境友好的合成工艺具有重要意义。基于Fe(III)在以H₂O₂为氧化剂的选择性氧化反应中优异的催化活性^[15,16], 以及金属离子在预组装过程中对分子印迹聚合物催化剂稳定性及催化活性的调控作用, 我们采用分子印迹技术, 分别以*o*-、*m*-和*p*-硝基苯甲醇(NBA)与FeCl₃的配合物为模板分子, 在分子印迹空腔内构建Fe(III)催化活性中心, 设计并制备了对应的分子印迹聚合物负载Fe(III)催化剂*o*-Fe(III)-MIP, *m*-Fe(III)-MIP和*p*-Fe(III)-MIP, 并考察了它们以水为溶剂, 30% H₂O₂为氧化剂的苯醇类选择性氧化反应中的催化活性和底物识别性。

2. 实验部分

2.1. Fe(III)-MIP的制备

o-NBA, *m*-NBA, *p*-NBA, 丙烯酰胺(AM), 二乙烯基苯和二甲基丙烯酸酯(EGDMA)为Alfa Aesar试剂, FeCl₃, 偶氮二异丁腈(AIBN), 二甲基亚砜(DMSO)和甲苯为国产试剂。反应溶剂经NaH或CaH₂除水后使用。

分子印迹聚合物Fe(III)-MIP的制备如图式1所示。将0.525 mmol无水FeCl₃和0.75 mmol *o*-NBA加入到5 ml甲苯与5 ml DMSO的混合溶液中, 振荡静置, 再加入3 mmol AM, 15 mmol EGDMA和0.1 g AIBN, 充分振荡摇匀, 将溶液转移至20 ml硬质试管中, 超声, 通N₂15 min除O₂, 真空封管, 60 °C热引发聚合24 h。聚合物脱除溶剂后研磨并过200目筛, 用丙酮(9 ml)倾析3次, 用甲醇和乙酸(体积比9:1)混合液作洗脱液, 索氏提取洗脱模板分子, 直至洗脱液中用紫外光谱检测不出模板分子。洗脱后, 于40 °C真空干燥聚合物, 得到分子印迹聚合物负载的Fe(III)催化剂, 记为*o*-Fe(III)-MIP。此外, 分别以*m*-NBA及*p*-NBA与无水FeCl₃的配合物为模板分子, 同法制备*m*-Fe(III)-MIP和*p*-Fe(III)-MIP。采用络合滴定法, 测定上述三个催化剂中Fe(III)含量基本相同, 约为0.030 mmol/g。

为了比较, 还制备了空白的非印迹聚合物(NIP)以及该非印迹聚合物负载的Fe(III)催化剂(Fe(III)-NIP), 制备过程除不加模板分子外, 其它操作与*o*-Fe(III)-MIP相同。

2.2. 催化剂铁含量的测定

称取约0.1 g催化剂, 在500–600 °C焙烧5 h, 除去催化剂中的有机成分, 将剩余的铁氧化物转移到锥形瓶中, 加入4 ml王水, 煮沸至干, 处理3次。加入5 ml蒸馏水将

固体溶解, 后加入10 ml氨基乙酸-盐酸缓冲溶液, 调节pH=2–3, 加入5滴碘基水杨酸(100 g/L), 所得溶液加热到60 °C, 用EDTA溶液(0.01 mol/L)滴定至酒红色消失。平行滴定3次, 取平均值^[16]。

2.3. FeCl₃与功能单体及模板分子间相互作用的监测

在常温下, 取2.5 ml模板溶液于紫外-可见光谱仪吸收池中, 每次取100 μl功能单体溶液滴入模板溶液中, 通过测量每次滴定后溶液吸光度的变化来监测模板分子与功能单体的相互作用。类似地, 分别将功能单体和模板溶液加入到FeCl₃溶液中, 并测量每次混合后溶液的紫外吸光度^[17]。

2.4. 催化剂的表征

催化剂形貌用JSM-6360LV型扫描电子显微镜(SEM)观察。样品的比表面积和孔结构在Micromeritics TriStar 3000型物理吸附仪上于–196 °C测定, 样品在80 °C下抽真空预处理至压力小于1 × 10^{–3} Pa, 比表面积采用BET法计算, 孔径分布采用BJH方程计算。红外光谱(FT-IR)测定在AVATAR 370型红外光谱仪上进行, 扫描范围4000–400 cm^{–1}, 分辨率2 cm^{–1}。紫外-可见(UV-vis)吸收光谱在Perkin Elmer公司Lambda 19型UV-vis光谱仪上测定, 波长范围200–600 nm。

2.5. 催化剂性能测试

在50 ml圆底烧瓶中依次加入0.1 g Fe(III)-MIP, 1.8 mmol NBA和15 ml去离子水, 调节溶液pH值为2, 搅拌下加热至80 °C。将0.75 ml过氧化氢(30%)用5 ml去离子水稀释后, 以0.1 ml/min的速度缓慢滴入反应体系中。反应完成后, 冷却至室温, 用乙醚萃取3次, 合并有机相, 用无水Na₂SO₄干燥。产物采用HP 5790型GC-MS仪定性, 用Agilent 6890型气相色谱仪定量分析。

3. 结果与讨论

3.1. Fe(III)-MIP的设计

模板分子与功能单体之间的自组装是构建印迹空穴的前提。经过模板与单体的相互诱导, 单体的功能基团定向地排列在模板周围, 形成一个高度有序的组织结构。金属离子与模板分子预组装, 使功能单体和与模板分子通过金属与之形成的配位键连结起来, 加强了功能单体与模板间的偶合作用。

以*p*-Fe(III)-MIP的设计为例。在FeCl₃溶液(0.2 mmol/L)中加入相同浓度的*p*-NBA, 观察混合溶液的UV-vis光谱变化, 见图1(a)。可以看出, 当FeCl₃与模板分子*p*-NBA等摩尔混合时, 溶液在285 nm处出现吸收峰。

随着

-NBA用量增加,该峰发生位移,且吸光度逐渐增加。这表明 FeCl_3 与

-NBA之间发生了相互作用。根据 FeCl_3 和

-NBA的结构,两者之间的作用应该是配位组装。当

-NBA加入量为 FeCl_3 的5倍时,特征紫外吸收波长达到最大为290 nm。进一步加入

-NBA,特征紫外吸收峰强度增加而波长没有变化。因此, FeCl_3 与

-NBA之间实现较好程度配位组装的化学计量比为1:5。

在 FeCl_3 溶液(0.2 mmol/L)中加入相同浓度的功能单体AM,观察它们之间的相互作用对UV-vis光谱的影响,结果见图1(b)。当AM/ FeCl_3 摩尔比为2:1时,混合溶液在271 nm处出现吸收峰,且随着混合溶液中AM量的增加而发生移动。该结果证实了 FeCl_3 除了与

-NBA之间存在鳌合作用外,还与功能单体AM之间存在相互作用。当AM/ FeCl_3 摩尔比为8:1时,特征紫外吸收波长达到最大为274 nm;进一步增加AM用量,特征紫外吸收峰吸光度增加但其位置不变。因此,AM与 FeCl_3 之间实现完全程度组装的摩尔比为8:1。

在

-NBA溶液(0.2 mmol/L)中加入相同浓度的AM,观察混合溶液的UV-vis光谱变化,结果见图1(c)。可以看出,当AM与

-NBA等量混合时,混合溶液在216 nm处出现吸收峰。当AM与

-NBA摩尔比增至4:1时,该吸收峰逐渐位移至219 nm,证明两者自组装相互作用达到饱和;进一步增加AM用量,吸光度增加,但吸收峰位置没有明显变化。因此,AM与模板分子

-NBA之间实现完全程度组装的摩尔比为4:1。

综上可见,单体与模板、单体与金属、模板与金属之间存在较强的相互作用,并且当增加单体或模板至一定量时,这种相互作用达到饱和。过高的单体用量会造成印迹聚合物周围结合位点过剩,导致结合位点与模板空间排列不对称;而单体用量过低则使印迹聚合物中结合位点数目过少,无法保证完全程度的分子自组装。因此,只有化学计量的单体才能提供完全程度的自组装。本文合成的MIPs催化剂中AM用量3 mmol, p-NBA用量0.75 mmol, FeCl_3 用量0.525 mmol。

3.2. 催化剂表征

3.2.1. SEM表征结果

图2为

-Fe(III)-MIP, Fe(III)-NIP和NIP样品的SEM照片。可以看出,p-Fe(III)-MIP具有明显的表面空腔结构。这是由于聚合过程中受 FeCl_3 和p-NBA的共同影响,生成的聚合物颗粒无定形化且不能整齐堆积,从而形成了堆积型空腔。这种堆积型空腔与洗脱模板分子后留下的印迹空穴相互贯通,有利于反应物分子在聚合物内的

扩散并且选择性吸附。不加模板分子的Fe(III)-NIP,由于聚合过程中不受模板分子的影响,洗脱后表面较光滑,且空腔数量较少。而空白印迹聚合物NIP经洗脱后,表面光滑,未见明显的空腔结构。结果表明,以p-NBA与 FeCl_3 络合物为模板分子,不仅可以在聚合物结构中构建空间立体结构和结合位点上与模板分子完全匹配的印迹空穴,而且可以在聚合物表面形成与之互穿的堆积型空腔,有利于提高MIPs的底物吸附能力。

3.2.2. N_2 吸附-脱附结果

图3为p-Fe(III)-MIP, Fe(III)-NIP和NIP样品的 N_2 吸附-脱附等温线及孔径分布曲线。由图可见,p-Fe(III)-MIP和Fe(III)-NIP样品等温线均为典型的IV型,特别是p-Fe(III)-MIP的吸附曲线在低压区($p/p_0 < 0.4$)上升较快,表明存在有一定数目的微孔(孔径<1.9 nm)。当 $0.4 < p/p_0 < 0.8$ 时,这两种材料的 N_2 等温线存在一个滞后环,表明存在部分介孔^[18,19],发生了毛细凝聚,使吸附量进一步增加。正如图3(b),p-Fe(III)-MIP和Fe(III)-NIP材料中均存在孔径为4.0 nm左右的介孔。当 $p/p_0 > 0.9$ 时,吸附量开始大量增加,这可能是无定形聚合物颗粒形成了堆积孔导致的。NIP样品则不具有明显孔道结构。表1给出了上述样品的织构性质。可以看出,p-Fe(III)-MIP的孔径、孔体积和比表面积均高于Fe(III)-NIP。其中比表面积几乎为Fe(III)-NIP的2倍。这表明p-Fe(III)-MIP催化剂聚合过程中受 FeCl_3 和p-NBA的共同影响,导致表面空腔较大。这与SEM结果一致。

3.2.3. FT-IR结果

图4为模板分子p-NBA,空白聚合物NIP, Fe(III)-NIP, p-Fe(III)-MIP以及未脱除模板分子的p-Fe(III)-MIP前体的FT-IR谱。可以看出,样品于3400–3700, 2700–3200和1500–1800 cm^{-1} 处出现的吸收峰分别归属于N-H/C-H, C=N和C-N的伸缩振动^[20];另外在指纹区主要是C-C旋转振动吸收带^[21]。模板分子p-NBA在3510 cm^{-1} 处出现醇羟基特征吸收峰;而在p-Fe(III)-MIP前体中,该特征吸收峰移到3443 cm^{-1} 处,证实在聚合过程中模板分子的醇羟基与金属离子之间形成了金属配位键。经甲醇和乙酸(体积比9:1)混合液索氏提取脱除模板分子后,该特征峰消失,表明模板分子被洗脱。p-Fe(III)-MIP, NIP和Fe(III)-NIP的FT-IR谱基本一致,表明脱除模板剂的过程没有破坏聚合物的结构。

3.3. 不同催化剂的催化活性

3.3.1. 单一NBA氧化反应

表2为各样品在以水为溶剂,过氧化氢为氧化剂的

o-NBA, *m*-NBA或*p*-NBA氧化反应中的催化性能。由表可见,无催化剂或以空白聚合物NIP为催化剂时,反应几乎不能发生。当以Fe(III)-NIP或Fe(III)-MIP为催化剂时,NBA氧化生成苯甲醛的活性明显提高。比较而言,Fe(III)-MIP催化剂表现出明显的底物识别性。以*o*-NBA为底物时,*o*-Fe(III)-MIP的催化活性最高,80 °C反应4 h,底物转化率为65%;而相同反应条件下,*m*-Fe(III)-MIP,*p*-Fe(III)-MIP和Fe(III)-NIP的催化活性相当,底物转化率仅为34%–39%。滴定法测定结果发现,这四种催化剂中Fe含量没有明显差别,约为0.030 mmol/g。因此,造成催化剂活性差别的原因应与其印迹空腔结构有关,*o*-Fe(III)-MIP中含有与底物(*o*-NBA)结构相同的印迹空腔和识别位点,有利于选择性地吸附底物,因此可提高催化剂活性^[22,23]。*m*-Fe(III)-MIP,*p*-Fe(III)-MIP 和Fe(III)-NIP结构中没有与*o*-NBA结构匹配的印迹空腔和识别位点,因此在*o*-NBA氧化反应中的催化活性远低于*o*-Fe(III)-MIP。*m*-Fe(III)-MIP对*m*-NBA氧化反应表现出较高的催化活性,底物转化率可达69%;而以*o*-Fe(III)-MIP,*p*-Fe(III)-MIP 和Fe(III)-NIP为催化剂时,底物转化率仅为33%–42%。同样地,*p*-Fe(III)-MIP对*p*-NBA表现出较高的催化活性。由此可见,在以底物分子为模板设计的分子印迹聚合物印迹空穴内构建催化活性中心可使催化剂具有独特的底物识别性能,能加速识别分子的反应速率,提高活性。负载Fe(III)的非印迹聚合物Fe(III)-NIP因结构中没有与底物分子匹配的印迹空穴,在各NBA氧化反应中均不具有底物识别性能。

3.3.2. 混合NBA氧化反应

表3为*o*-Fe(III)-MIP,*m*-Fe(III)-MIP 和*p*-Fe(III)-MIP样品在*o*-NBA,*m*-NBA和*p*-NBA等量混合物氧化反应中的催化性能。由表可见,当以*o*-Fe(III)-MIP为催化剂时,*o*-NBA的转化率最高,80 °C反应4 h为70%。而其它两种NBA转化率相当,且明显更低。*o*-Fe(III)-MIP具有与混合底物中的*o*-NBA结构相同的印迹空腔和识别位点,有利于选择性地吸附*o*-NBA;而其它两种NBA中没有与*o*-Fe(III)-MIP结构匹配的印迹空腔和识别位点,其转化率较*o*-NBA的低。同样地,*m*-Fe(III)-MIP对混合底物中的*m*-NBA表现出较高的催化活性,底物转化率可达72%,而*o*- 和*p*-NBA的转化率分别仅为27% 和32%。此外,*p*-Fe(III)-MIP对混合底物中的*p*-NBA表现出较高的催化活性,其转化率可达85%,而催化*o*- 和*m*-NBA的转化率分别仅为29% 和40%。这进一步证实了以底物分子为模

板的分子印迹聚合物具有独特的底物识别性能。

3.3.3. 反应时间的影响

分别以*o*-,*m*-和*p*-NBA为底物,考察了反应时间对*o*-Fe(III)-MIP,*m*-Fe(III)-MIP和*p*-Fe(III)-MIP催化性能的影响,结果见图5。可以看出,具有不同印迹空穴的Fe(III)-MIP在反应过程中均表现出明显的底物识别性能。随着反应时间的延长,NBA的转化率均急剧增大,底物识别性能也越来越明显。反应4 h时,印迹效应达到最大。以*o*-NBA为底物时,*o*-Fe(III)-MIP催化活性最高,反应4 h *o*-NBA的转化率为65%,而*m*-Fe(III)-MIP 和*p*-Fe(III)-MIP上仅分别为39% 和36% (*o*-Fe(III)-MIP与*m*-Fe(III)-MIP催化活性的比率为1.67,*o*-Fe(III)-MIP与*p*-Fe(III)-MIP催化活性的比率为1.81)。延长反应时间至6 h,*o*-Fe(III)-MIP上*o*-NBA转化率增至72%,而底物识别性能有所下降(*o*-Fe(III)-MIP与*m*-Fe(III)-MIP催化活性的比率为1.44,*o*-Fe(III)-MIP与*p*-Fe(III)-MIP催化活性的比率为1.38)。这可能是因为时间延长有利于底物扩散,使不能与聚合物印迹空穴匹配的底物进入聚合物空穴与催化活性位接触,从而降低了印迹空穴的底物识别性能。值得注意的是,以*o*-NBA为底物时,*m*-Fe(III)-MIP 和*p*-Fe(III)-MIP均因不具有与底物匹配的印迹空穴而表现出类似的催化活性。以*m*-NBA为底物时,*m*-Fe(III)-MIP催化活性最高,反应4 h转化率为69%;而*o*-Fe(III)-MIP 和*p*-Fe(III)-MIP活性相当,反应4 h时*m*-NBA转化率分别为37% 和42%。同样地,在*p*-NBA氧化反应中,*p*-Fe(III)-MIP表现出最高的催化活性,反应4 h时其转化率达到80%;而*o*-Fe(III)-MIP 和*m*-Fe(III)-MIP催化剂上的转化率分别为58% 和49%。这进一步说明制备的Fe(III)-MIP催化剂具有与相应底物完全匹配的刚性空腔结构及与底物官能团互补的结合位点,因此在反应过程中表现出高效专一的底物识别性。

4. 结论

分别以*o*-,*m*-和*p*-NBA与FeCl₃的配合物为模板,制备了对*o*-,*m*-和*p*-NBA有底物识别性的分子印迹催化剂*o*-Fe(III)-MIP,*m*-Fe(III)-MIP 和*p*-Fe(III)-MIP。在以水为溶剂,过氧化氢为氧化剂的苯甲醇衍生物的催化氧化反应中,该类催化剂不仅具有优异的催化活性,而且表现出特殊的底物识别性能。因此,该催化剂具有预见性和可控性,可为一些特殊结构底物的催化氧化反应设计专有催化剂提供新思路。